Electron excitation cross sections for the metastable and resonant levels of Ne($2p^5 3s$)

Mark H. Phillips,* L. W. Anderson, and Chun C. Lin
Department of Physics, University of Wisconsin, Madison, Wisconsin 53706
(Received 11 February 1985)

The electron excitation cross section both for the $^3P_2$ and $^3P_0$ metastable levels ($1s_5$ and $1s_3$ in Paschen's notation) and for the mixed $^3P_1$ and $^1P_1$ resonant levels ($1s_4$ and $1s_2$ in Paschen's notation) of the $2p^5 3s$ configuration of Ne have been measured. Apparent and direct excitation cross sections are reported for incident electron energies from threshold to 300 eV and are compared with results of different methods of measurements. Ground-state Ne atoms are excited by a monoenergetic electron beam to the $1s$ levels, and atoms in the $1s$ levels are pumped to the $2p$ levels of the $2p^5 3p$ configuration by means of a cw dye laser. The laser-induced fluorescence from the $2p$ level is utilized to determine the electron excitation cross section for the $1s$ level. Methods for absolute calibration of the cross sections are given.

I. INTRODUCTION

Studies of the electron-impact excitation of Ne atoms are of special importance in understanding the basic physics of collisional excitation processes and in technological applications. The Ne atom has a large number of excited levels. The magnitude and the energy dependence of the excitation cross sections vary widely among these levels.[1] Experimental measurements of the cross sections have led to the development of a theoretical scheme for characterizing the excitation cross sections that successfully explains, on a semiquantitative level, the observed excitation data.[1] In addition to its fundamental interest, Ne plays an important role in many discharges such as Ne-discharge light sources, the He-Ne laser, and the Ne-Xe-NF_2 laser.[2] Knowledge of the excitation cross sections is essential for modeling discharges that contain Ne.

The ground level of Ne is $1s^2 2s^2 2p^6\ ^1S_0$. The lowest excited configuration $1s^2 2s^2 2p^5 3s$ consists of four energy levels as shown in Fig. 1. These levels, which are called $1s_2$, $1s_3$, $1s_4$, and $1s_5$ in Paschen's notation, have total angular momentum J of 1, 0, 1, and 2, respectively. The $1s_3$ and $1s_5$ levels are, respectively, nearly pure $^3P_0$ and $^3P_2$ levels and are metastable with very long radiative lifetimes. The $1s_2$ and $1s_4$ levels, with $J=1$, have wave functions that are linear superpositions of the LS-coupling $^1P_1$ and $^3P_1$ eigenfunctions. The $1s_2$ level is primarily $^1P_1$ in character with a small (less than 10%) admixture of $^3P_1$, and vice versa for the $1s_4$ level. Measurements of the lifetime of the $1s_2$ level are in agreement with a value of about 1.65 nsec.[3] The $1s_4$ level is optically connected to the ground level through the $^1P_1$ admixture so that its radiative decay rate is small compared to that of the $1s_2$ level. The measured lifetimes of the $1s_4$ level cluster about two different values, 21 and 30 nsec.[3] We adopt the value of 20.5 nsec, obtained by Bhasker and Lurio,[3] since their experiment was performed with careful attention to eliminating cascade effects. At "high" Ne densities (above 3×10^{14} atoms/cm^3) the radiation from the $1s_2$ and $1s_4$ resonance levels is trapped so that the effective lifetimes of these levels are much longer than the radiative lifetimes of isolated atoms.

In the experiments of Sharpton *et al.*[1] the excitation cross section for a given level is determined by measuring the intensity of photon emission from that level. The electron excitation cross sections of the $1s_3$ and $1s_5$ levels cannot be measured by this optical method since these levels are metastable and do not radiate. We have used a laser-induced fluorescence technique to measure the elec-

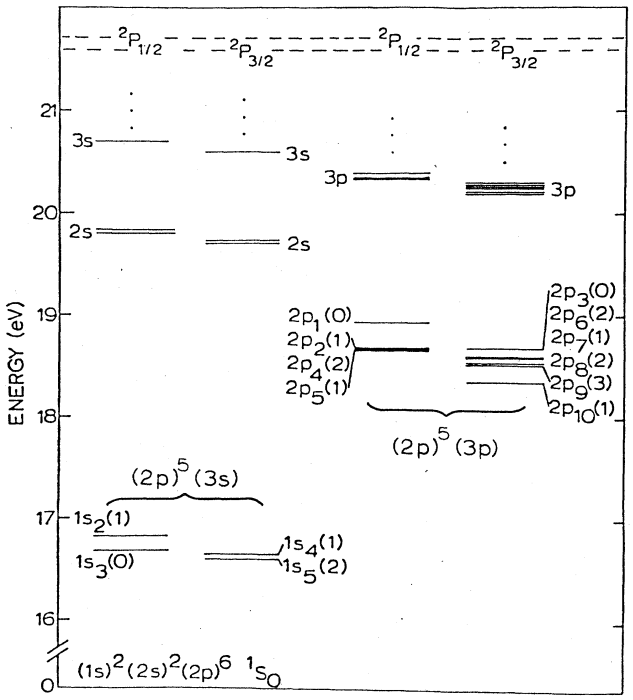

FIG. 1. Energy levels associated with the ground, $(2p)^5(3s)$, and $(2p)^5(3p)$ configurations of the neon atom. A symbol like $1s, 2s, 2p, \ldots$, without parentheses around it labels an energy level in Paschen's notation. The numeral inside parentheses after $1s_1, \ldots, 1s_4$, $2p_1, \ldots, 2p_{10}$ refers to the value of the total angular momentum J.

tron excitation cross section of the $1s_3$ and $1s_5$ levels.[4,5] Although the electron excitation cross sections of the $1s_2$ and $1s_4$ levels can be determined using the optical method, an experimental difficulty arises in connection with photon-intensity measurement because of the very short wavelength (746 Å) of the radiation they emit. At sufficiently high atom density the lifetimes of the $1s_2$ and $1s_4$ levels are increased by radiation trapping so much that they become similar to metastable levels. Thus we have also been able to use the laser-induced fluorescence technique to measure the $1s_2$ and $1s_4$ cross sections.[6] Preliminary reports of measurements of the electron excitation cross sections of the four $1s$ levels using laser-induced fluorescence are given in Refs. 4—6. In this paper we present a more detailed account for the experimental apparatus, data analysis, and discussion of the results. There have been a number of previous measurements of the electron excitation cross sections of one or several of the $1s$ levels of Ne. A comparison of our results with those of the previous works is given in Sec. IV of this paper. We have also measured the excitation cross sections for each of the Zeeman sublevels of the $1s_5$ level.[7] These measurements are not discussed in this paper.

II. EXPERIMENTAL APPARATUS

Figure 2 shows a schematic diagram of our apparatus.[4,6] A collimated monoenergetic electron beam passes through a chamber filled with Ne gas at a pressure of 1—40 mTorr, exciting some of the Ne atoms to one of the $1s$ levels. A cw dye-laser beam passes through the chamber intersecting and perpendicular to the electron beam. The laser wavelength is set to the transition between one of the $1s$ levels denoted by a and one of the ten levels of the $2p^5 3p$ configuration (the $2p$ levels in Paschen's notations) denoted by b. Some of the atoms excited by the electron beam to level a absorb a laser photon and are excited to level b. The b-level atom decays radiatively to one of the $1s$ levels (denoted as level c) other than level a. This is illustrated in Fig. 3. The laser-induced fluorescence emitted as the Ne atom decays from level b to level c is detected along an axis that is mutually perpendicular to the electron beam axis and the dye-laser beam axis. As is discussed in Sec. III of this paper, the rate of formation of excited atoms in state a, which is directly proportional to the apparent excitation cross section, is determined from the intensity of the laser-induced fluorescence. The apparatus has four basic parts: the vacuum system, the electron gun, the laser, and the fluorescence-detection system. They are described in the following paragraphs.

The vacuum system is composed of a collision chamber and a gas-handling system. The vacuum system is made of stainless steel and is sealed with copper gaskets. Pyrex windows permit radiation to exit the vacuum system. The vacuum system is evaluated to a pressure of about 1×10^{-7} Torr prior to introducing Ne. The Ne used has a purity greater than 99.9%. Typical operating neon pressures are 1 to 36 mTorr (densities of 3.6×10^{13} to 1.3×10^{15} atoms/cm^3) as measured with a capacitance manometer. A getter pump maintains the background pressure at about 10^{-6} Torr without measurably affecting the Ne pressure.

The electrostatic focusing electrodes of the electron gun are made of stainless steel and are mounted on one end of the collision chamber. The gun has an indirectly heated cathode. The electron beam is collimated with a typical diameter of 2 mm. Laser-induced fluorescence measurements are made with electron-beam energies ranging from below threshold to greater than 300 eV and with beam currents in the range of 50-500 μA. The collision region is inside a grounded Faraday cup. Apertures in the Faraday cup allow the Ne radiation to be observed and the laser beam to enter and exit. The slits are perpendicular

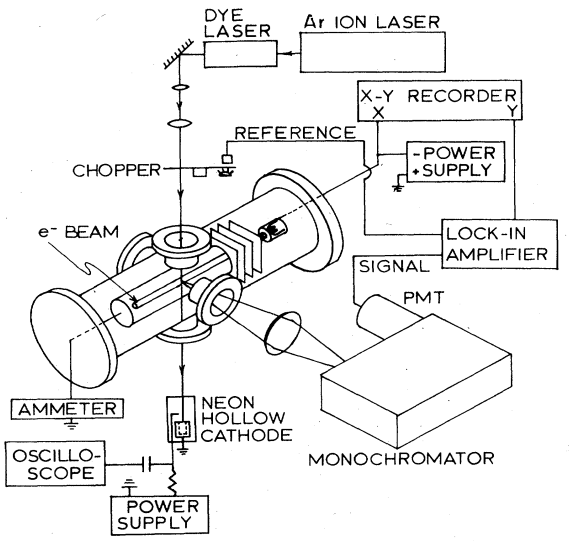

FIG. 2. Schematic diagram of the apparatus used in this work.

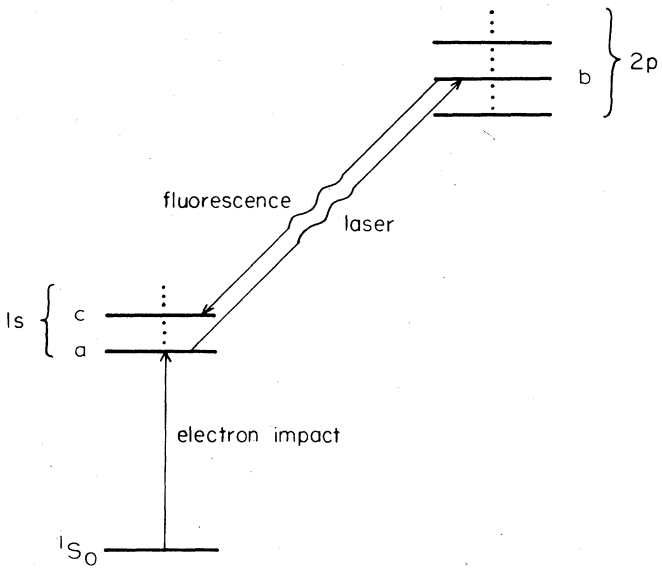

FIG. 3. A diagram showing the processes of excitation by electron impact, excitation by absorption of laser radiation, and emission of fluorescence radiation.

to the electron beam and are parallel to the laser beam and are long enough that one views a region 5 times as wide as the width of the electron beam. The electron beam, as it passes through the observation region, is already inside the Faraday cup so that the entire electron beam is collected except for that part of the beam that is scattered out the observation slits or backscattered out the entrance aperture. The slits occupy only about 3% of the area of the cylinder that forms the side of the Faraday cup. Since our measurements show that only a small part of the current hits the side of the Faraday cup, less than 1% of the electron beam can be scattered out the slits. The entrance to the Faraday cup is through a plate. The area of the hole is about 5% of the area of the plate. The backscattered current to the plate is found to be about 1% of the total current with high Ne pressure. Thus the electron beam scattered out the aperture must be much less than 1%. We conclude that we collect essentially all the electron beam that excites the Ne in the observation region. As further evidence of this, we have measured the apparent excitation cross sections of the Ne $2p$ levels. Our measured apparent cross sections are independent of the pressure and are identical to the cross sections measured by Sharpton *et al.* at pressures even lower than we use. The electron current to the Faraday cup is measured with an electrometer. The electrometer provides an analog output voltage proportional to the electron-beam current. As will be shown in Sec. III, the laser-induced fluorescence intensity is directly proportional to the apparent electron excitation cross section, the neon-gas density and the electron current density. The electron current density is proportional to the electron current if the electron-beam diameter is constant.

The energy spread of the electron beam is measured using the sharp peak corresponding to the negative-ion resonance in the curve of the $2p_{10}$ electron-excitation cross section versus energy. The intrinsic energy width of this resonance[8] is less than 0.2 eV which is narrower than the energy distribution of our electron beam. The observed energy width of the $2p_{10}$ cross-section resonance in excess of 0.2 eV is due to the spread of the energies of the electrons in the electron beam. The energy spread of the electron beam determined in this manner is 0.5 eV full width at 20% of maximum. The energy spread of the electron beam is also determined to be about 0.5 eV using the abruptness of the onset of the excitation functions.

Contact potentials and the charging of plates in the electron gun cause the true electron energy in the collision region to differ from the energy calculated using the applied voltages by an offset voltage. The offset voltage is determined by comparison of the measured values of the threshold voltage for the onset of the electron excitation with the expected voltages calculated from the atomic energy levels. Charging of the plates is probably due to formation of a dielectric film caused by polymerization of pump oil as a result of electron impact. A freshly cleaned electron gun yields a voltage offset of about 1 V. The offset increases by 2—3 V over a period of two months with constant use. We observe the same offset for selected lines of Ne, He, and He^+. Thus we conclude that the offset is independent of electron energy even through the offset is gradually changing.

The laser system consists of a cw tunable dye laser pumped by an Ar-ion laser. The cw dye laser is a broadband multimode standing-wave tunable dye laser. The dye laser has a range of output wavelengths from 570 to 750 nm using R6G, DCM, and LD700 dyes. Powers greater than 100 mW are possible over the entire wavelength range. A beam-expanding telescope permits adjustment of the diameter of the laser beam from 1.5 to 3 mm. The laser beam is mechanically chopped at 720 Hz before it enters the collision chamber. The longitudinal cavity modes are separated by 4.2×10^8 Hz. The measured bandwidth of the laser is 1.5×10^{10} Hz for a given setting of the birefringent tuning filter so that lasing can occur on about 35 cavity modes. Mode competition may prevent simultaneous lasing on all of the modes. The particular modes that are lasing may vary in time. We do not know the exact number and frequencies of the lasing modes, nor the exact time dependence of the lasing modes. In Sec. III, we discuss the effects of this multimode-laser output on the measurement of the cross sections.

The laser beam upon exiting the collision chamber is directed into a neon hollow-cathode discharge. Detection of the optogalvanic effect in the discharge is used to set the dye-laser wavelength to the wavelength of the appropriate transition from level a to b.

The Ne radiation emitted at right angles to both the electron beam and the laser beam exits the collision chamber through a Pyrex window. The radiation is collected and focused by a lens onto the entrance slits of the 1-m Jobin-Yvon monochromator. Measurements are made typically with a monochromator resolution of 2 Å. A pair of slits parallel to the image of the electron beam and perpendicular to the monochromator slits can be mounted on the monochromator entrance slit. By translating these slits in a direction perpendicular to the image of the electron beam, the spatial variation of the electron beam is measured.

The detection of the radiation is accomplished with a low-noise, cooled photomultiplier tube (PMT) and a lock-in amplifier. The output current from the PMT is the input for the lock-in amplifier. The reference signal for the lock-in amplifier is obtained from the mechanical chopper which modulates the laser intensity. The output voltage signal of the lock-in amplifier is divided by the analog voltage proportional to the electron-beam current, and the quotient is applied to the y axis of the x-y recorder; the x axis is the electron-gun accelerating voltage. The resultant plot is used to determine the apparent excitation cross section of the $1s$ level a as a function of incident electron energy.

III. METHODS OF MEASUREMENTS

A. Relation between the laser-induced-fluorescence signal and excitation cross sections

Using the rate equations for the population of levels a and b, we have shown[4] that the density of atoms in level b with laser on, $n_{b\text{-on}}$, is

$$n_{b\text{-on}}=\frac{nJ}{e}\frac{Q_b^A+\alpha(Q_a^A-Q_{ba})}{A_b+\alpha(-A_{ba}+g_aA_a/g_b)}\ , \tag{1}$$

$$\alpha=B_{ab}\rho(\nu)/[B_{ab}\rho(\nu)+A_a]\ , \tag{2}$$

where n is density of ground-level atoms, J is the electron-beam current density, e is the proton charge, g_a and g_b are the statistical weights of levels a and b, A_{ba} and B_{ab} are the Einstein coefficients, $\rho(\nu)$ is the energy density of radiation of frequency ν in the laser beam, A_a and A_b are the reciprocals of the lifetimes for levels a and b. For the metastable levels A_a^{-1} is not the radiative decay time, but is the time that an electron at thermal velocities spends in the laser beam. For the resonant levels A_a^{-1} is the time during which the excitation is kept in the laser beam by radiation trapping. The optical cross section Q_{ij} for the $i\rightarrow j$ transition is defined by

$$Q_{ij}=(n_iA_{ij})/(nJ/e)\ , \tag{3}$$

and is merely a notation for expressing radiative emission into level j from a higher level i in the form of a cross section. The apparent cross section of level i, Q_i^A, is the sum of the cross section for populating level i by direct electron impact and by cascades from higher levels and is given by

$$Q_i^A=Q_i+\sum_{j\,(>i)}Q_{ji}\ , \tag{4}$$

where Q_i is the direct electron excitation cross section and where the second term is called the total cascade cross section.

When the laser is blocked off from entering the collision chamber, the population of level b, $n_{b\text{-off}}$, is due solely to direct electron impact and cascade and is given by

$$n_{\text{b-off}}=(nJ/e)(Q_b^A/A_b)\ . \tag{5}$$

The Doppler width of the $1s\rightarrow 2p$ ("a"$\rightarrow$"b") transition in Ne is approximately 1 GHz. This is much narrower than the bandwidth of the laser. The standing-wave laser is a multimode laser; the exact lasing frequencies and the exact time dependence of the mode intensities are not known. $\rho(\nu)$ is neither constant in frequency nor constant in time and the stimulated transition rate $B_{ab}\rho$ is a function of the time. Therefore, the signal measured with the laser on S_{on} which is proportional to $n_{b\text{-on}}$, involves a time average over the quantity α. When the laser is blocked off, S_{off} is proportional to $n_{b\text{-off}}$. The output signal from the lock-in amplifier is proportional to the difference between the signal when the laser is on and when it is off

$$\begin{aligned}S_{\text{on}}-S_{\text{off}}&=K(n_{b\text{-on}}-n_{b\text{-off}})\\&=K\frac{nJ}{e}\left\langle\frac{\alpha(Q_a^A-Q_b^Ag_aA_a/g_bA_b)}{A_b+\alpha(-A_{ba}+A_ag_a/g_b)}\right\rangle\ ,\end{aligned} \tag{6}$$

where K is a constant of proportionality and where the angular brackets indicate the average over the time of measurement.

When the frequency ν is the same as that of a laser mode and when ν is within the Doppler line profile of the a-to-b absorption, then $\alpha\simeq 1$. To see this let us consider the particular example of the $1s_5\rightarrow 2p_2$ absorption and with a dye-laser power of 100 mW. The photon flux in a 1-mm-diam laser beam is 3.8×10^{19} photons/cm^2 sec. Since there are at most 35 modes lasing, the flux per mode is at least 1.1×10^{18} photons/cm^2 sec which corresponds to $B_{ab}\rho\simeq 6\times10^6$ sec^{-1}. The transit time for a Ne atom to cross the laser-beam diameter is about 3×10^{-6} sec. At the pressures used in our experiment the distance an atom travels between collisions is greater than the diameter of the laser beam. Thus for the metastable atom $A_a\cong 3\times10^5$ sec^{-1}, so that $B_{ab}\rho\gg A_a$ and hence, $\alpha\simeq 1$ whenever a lasing mode interacts with a segment of the Doppler profile. The laser mode burns a hole in the Doppler profile of width $\Delta\nu=\Delta\nu_{\text{homo}}(1+I/I_s)^{1/2}$ where the homogeneous broadening $\Delta\nu_{\text{homo}}=(2\pi\tau_0)^{-1}\cong 8\times10^6$ sec^{-1}, τ_0 is the radiative lifetime of the $2p_2$ state, I is the laser intensity, and I_s is the saturation intensity. In our experiment, optical pumping occurs when atoms are optically removed from level a and do not return. When this type of optical pumping is important, the saturation intensity is approximately given by $I_s\simeq\hbar\omega/\sigma T$, where $\hbar\omega$ is the energy of the transition,[9] σ is the absorption cross section of a homogeneous packet at line center, and T is the time for a Ne atom to cross the laser beam. Thus for the $1s_5\rightarrow 2p_2$ absorption, $I_s\simeq 1$ mW/cm^2. The intensity I per mode is much higher than I_s for all our experimental situations so that $(1+I/I_s)^{1/2}\simeq(I/I_s)^{1/2}$. Similar results hold for all the transitions we have studied. Thus the signal comes from those atoms in the holes burned by the laser modes within the Doppler width of the a-to-b absorption so that

$$S_{\text{on}}-S_{\text{off}}=\frac{\beta\sqrt{I}}{A_b-A_{ba}}\left[Q_a^A-\frac{g_aA_a}{g_bA_b}Q_b^A\right]\ , \tag{7}$$

where β is a constant determined by the number of lasing modes under the Doppler profile, by the saturation intensity, and by the fraction of the time these modes are lasing. Here we have dropped the A_ag_a/g_b term in the denominator of Eq. (6) since $A_a\ll A_b$. Equation (7) is valid in the limit where the laser is intense enough to saturate an individual packet but is not intense enough to burn a hole as large as the width of the entire inhomogeneous line. Thus the measured signal is proportional to $Q_a^A-g_aA_aQ_b^A/g_bA_b$. The second term in this expression is much smaller than the first. To illustrate this we note that for the $1s_3$ and $1s_5$ levels $g_aA_aQ_b^A/g_bA_b$ is less than 1% of the cascade component of Q_a^A and hence less than 1% of Q_a^A. Similar results are true for the $1s_2$ and $1s_4$ levels. Therefore we drop the $g_aA_aQ_b^a/g_bA_b$ term, i.e.,

$$S_{\text{on}}-S_{\text{off}}=\beta\sqrt{I}Q_a^A/(A_b-A_{ba})\ . \tag{8}$$

Qualitatively the laser-induced-fluorescence experiment may be pictured in the following way. Metastable atoms are produced by the electron beam at a rate given by the apparent excitation cross section Q_a^A. If the intensity and bandwidth of the laser are such that the $a\rightarrow b$ transition is much faster than the metastable-level decay rate A_a over the entire absorption profile, practically all the metastable atoms produced by the electron-beam excitation are transported to the level b. The rate of production of

metastable atoms by the electron beam is then equal to the rate of population of the level b by the laser action, or is proportional to the rate of the laser-induced $b \rightarrow c$ fluorescence. Thus $S_{on} - S_{off}$ for the $b \rightarrow c$ emission is proportional to Q_a^A. The denominator $A_b - A_{ba}$ in Eq. (8) can be understood easily. In the absence of the laser, the population of a particular level by electron impact is equal to the apparent excitation cross section divided by the Einstein coefficient A, the sum of the radiative decay rates to all the lower levels. When the laser is tuned to the $a \rightarrow b$ absorption, the $b \rightarrow a$ emission is no longer a decay channel for the level b because each $b \rightarrow a$ transition is followed by laser pumping, returning the atom to the level b. The total radiative decay rate in this case is $A_b - A_{ba}$. In our experiment the laser is intense enough to saturate an individual packet of the absorption profile but not the entire profile. $S_{on} - S_{off}$ is still proportional to $Q_a^A/(A_b - A_{ba})$, but in addition is proportional to $\sqrt{I}$ as indicated in Eq. (8).

B. Absolute calibration

From our experiments and using Eq. (8) we obtain the energy dependence of Q_a^A. Because the quantity β in Eq. (8) is not known, we obtain the absolute calibration of Q_a^A as follows.

The cross sections for direct electron excitation from the $^1S_0$ ground level to $1s_3$ and $1s_5$, which are purely triplet levels, have peaks at energies slightly above the threshold energy and decrease rapidly with increasing incident electron energy.[10] The $2p$ levels (except $2p_9$) have wave functions that are linear superpositions of triplet and singlet wave functions, and their excitation cross sections at high energies have relatively large values and a slow decrease as energy increases.[1] At large energies the direct excitation cross section of the $1s_3$ and $1s_5$ levels is negligible compared to the total cascade cross section so that the apparent cross section of the $1s_3$ and $1s_5$ levels is nearly equal to the total cascade cross section. The energy dependence of our measured apparent excitation cross section for the $1s_3$ or $1s_5$ level agrees well with the energy dependence of the total cascade cross section into the $1s_3$ or $1s_5$ level reported in Ref. 1 at electron energies above 80 eV. The apparent cross sections for the $1s_3$ and $1s_5$ levels are normalized at 90 eV to equal $\sum_{j(>a)} Q_{ja}$ ($a = 1s_3, 1s_5$) using the measurements of Sharpton *et al.*[1]

The cross sections for direct electron excitation of the $1s_2$ and $1s_4$ levels have a broad peak and decline slowly with increasing energy.[1] Thus the absolute values of the $1s_2$ and $1s_4$ cross section cannot be obtained by the method used for the $1s_3$ and $1s_5$ cross sections. For the $1s_2$ and $1s_4$ levels the product of their direct excitation cross section calculated by using the Born approximation times the incident electron energy is proportional to a constant plus the logarithm of the incident electron energy.[11] For levels that are not optically connected to the ground level but are spin-allowed such as the $2p$ levels, the product of the direct excitation cross section calculated by using the Born approximation times the incident electron energy is equal to a constant.[11] Under the Born approximation, the apparent cross section of an optically allowed level has both the $(\log_{10}E)/E$-type and $1/E$-type terms. If we plot the product of E times the unnormalized data of Q_a^A for $1s_2$ and $1s_4$ levels versus $\log_{10}E$, we get a straight line down to an energy as low as 120 eV for both cases (Fig. 4). This verifies the validity of the Born approximation for energies above 200 eV for excitation of both the $1s_2$ and $1s_4$ levels. The cascade component ($\sum_{j>a} Q_{ja}$) of the apparent cross section is known from the absolute measurements of Ref. 1. The direct cross sections Q_a for both $1s_2$ and $1s_4$ have been calculated by Fajen using the Born approximation.[1,12] In the region where Q_a varies as $(\log_{10}E)/E$, the Born cross sections are proportional to the square of the same dipole matrix elements used in the calculation of the lifetime of the level. The same set of wave functions used for the Born cross section gives a lifetime[1] for the $1s_2$ level that is 36% larger than the experimental value of 1.65 nsec. Accordingly we correct the Born cross sections by a scale factor equal to the ratio of the measured lifetime to the calculated lifetime. Our normalization procedure is to set Q_a^A of the $1s_2$ level to the sum of the measured cascade (from Ref. 1) and the scaled Born cross section at 300 eV. When this is done we find that Q_a^A remains equal to the sum of the measured cascade and the scaled Born cross section from 300 eV down to 200 eV. This supports the validity of our calibration. The measured lifetime of the $1s_2$ level has a 10% uncertainty, and thus it contributes a 10% uncertainty to Q_a. Other sources of uncertainty in Q_a are discussed in Sec. IV of this paper. For the $1s_4$ level Fajen has calculated a lifetime that is about 39% larger than the measured lifetime of 20.5 nsec. Analogous to the $1s_2$ level, we scale the Born cross section for the $1s_4$ level by the ratio of the measured lifetime to the calculated lifetime and use the scaled Born cross section along with the measured cascade from Ref. 1 for normalizing the apparent cross section at 300 eV. The stated uncertainty in the measured $1s_4$ lifetime is $\pm 7.3\%$.

The direct excitation cross sections for electron energies from threshold to 300 eV are obtained by subtracting the previously measured cascade cross sections from our apparent cross sections. The direct excitation cross sections calculated by the Born approximation agree well with our values above 200 eV, indicating that 300 eV is an appropriate energy for normalization. Figure 4 also contains a plot of $Q_a E$ versus $\log_{10}E$ for the direct excitation cross sections of the $1s_2$ and $1s_4$ levels. These are linear above 150 eV, further substantiating the validity of the Born approximation at 300 eV.

IV. RESULTS AND DISCUSSION

A. Discussion of experimental method

Our measurements of the apparent and direct electron excitation cross sections[4–6] of the four $1s$ level of Ne are summarized in Tables I and II and Fig. 5. These cross sections were measured using various conditions. First, the cross section for each $1s$ level is measured using different $2p$ levels as the b level. For instance, $2p_1$, $2p_2$, and $2p_4$ are used for $1s_2$; $2p_2$, $2p_5$, and $2p_7$ for $1s_3$; $2p_2$, $2p_4$, $2p_5$, and $2p_8$ for $1s_4$; $2p_2$, $2p_4$, $2p_5$, and $2p_6$ for $1s_5$.

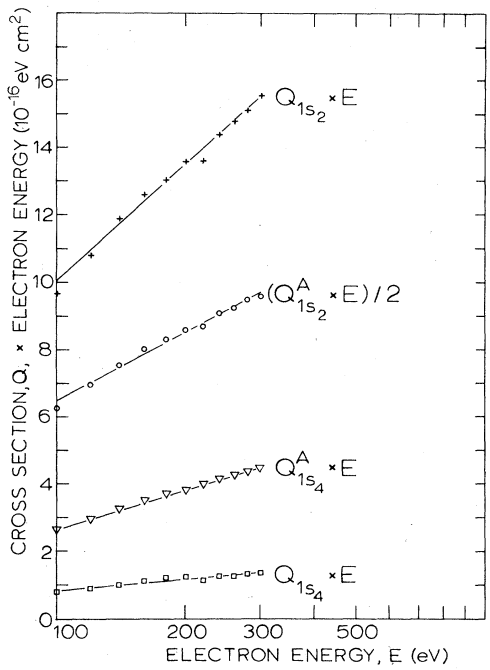

FIG. 4. Plots of the products of cross section times energy vs energy in logarithmic scale for the apparent excitation cross section (Q^A) and direct excitation cross section (Q) of the $1s_2$ and $1s_4$ levels.

Also different $1s$ levels are used as the c level. There is no measurable difference in the energy dependence of the excitation cross sections obtained for different b or c levels in the transition sequence. This supports our earlier conclusion that the second term in the numerator of Eq. (7) is much smaller than the first for all choices of the b level.

The laser-induced fluorescence is also a function of the cw dye-laser intensity. As indicated in Eq. (7) we expect $S_{on}-S_{off}$ to vary as the square root of the laser intensity I. We have observed the variation of $S_{on}-S_{off}$ with moderate laser intensity for a number of transitions and always find it varies as $\sqrt{I}$. For example, for the $1s_5 \rightarrow 2p_2$ transition the measured ratio of $S_{on}-S_{off}$ at $I=100$ mW to $S_{on}-S_{off}$ at $I=33$ mW is 1.79 ± 0.08.

One source of complication in our experiments is the change in current density when the electron energy is varied. This change is the result of a change in focusing characteristics of the electron gun as a function of electron energy. The diameter of the electron beam and the magnitude of the current depend on the electrode voltages. If the diameter of the electron beam remains less than that of the laser beam, then we observe no dependence of the laser-induced fluorescence signal on the laser-beam diameter or the electron-beam diameter. If the electron-beam diameter becomes larger than the laser-beam diameter, a spurious variation of Q_a^A with the individual electrode voltages is observed causing a distortion of the excitation function. As mentioned in Sec. II, a pair of horizontal slits, parallel to the electron beam, are mounted on the monochromator entrance slits. A profile of the electron beam is obtained by translating the horizontal slits. In this way, we determine settings for the voltages on the electron-gun elements that result in an electron beam that varies in diameter by no more than 20% as the electron accelerating voltage is varied. Under these conditions the electron beam is always smaller than the laser beam. We measure electron excitation cross sections for various electron-gun voltages, for which we obtain satisfactory electron-beam collimation. The results

TABLE I. Our measured values of the apparent (Q^A) and direct (Q) electron-impact excitation cross sections for the $1s_3$ and $1s_5$ levels of Ne in units of 10^{-19} cm^2 at different energies. Estimated uncertainty is 20% for the apparent excitation cross sections and 25% for the direct excitation cross sections.

E (eV)	$Q^A(1s_3)$	$Q(1s_3)$	$Q^A(1s_5)$	$Q(1s_5)$
25	5.8	1.8	33	10
30	6.0	1.4	31	7.3
35	5.8	1.1	30	5.4
40	5.7	0.93	29	4.1
50	5.5	0.61	26	2.3
60	5.2	0.42	24	
70	5.0		22	
80	4.8		20	

TABLE II. Our measured values of the apparent (Q^A) and direct (Q) electron-impact excitation cross sections for the $1s_2$ and $1s_4$ levels of Ne in units of 10^{-19} cm^2 at different energies. Estimated uncertainty is 25% for the apparent excitation cross sections and 28% for the direct excitation cross sections.

E (eV)	$Q^A(1s_2)$	$Q(1s_2)$	$Q^A(1s_4)$	$Q(1s_4)$
40	127	91	28	7.9
60	137	100	29	8.8
80	133	100	28	8.6
100	124	97	27	8.0
120	116	91	25	7.4
140	108	85	23	6.9
160	101	79	22	6.5
180	93	73	20	6.1
200	86	67	19	5.7
250	72	57	17	4.8
300	63	51	15	4.4

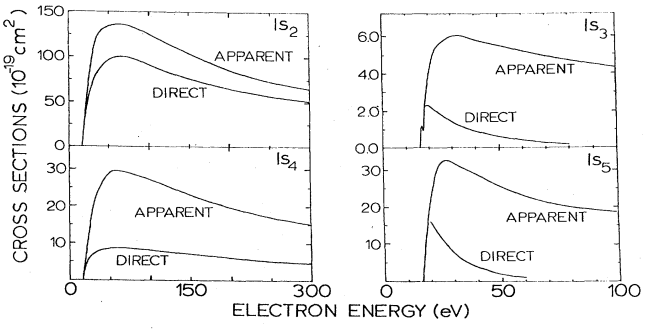

FIG. 5. Apparent and direct excitation cross sections of the $1s_2$, $1s_3$, $1s_4$, and $1s_5$ levels.

are reproducible with a random error of $\pm 10\%$.

In our experiment a cross-section area of the volume defined by the intersection of the electron beam and the laser beam is focused with unit magnification onto the entrance slits of the monochromator. The image of the laser beam is parallel to the entrance slits, so that the monochromator samples only part of the laser beam, if the monochromator slit width is less than the laser-beam diameter. The $2p$-to-$1s$ transition in the absence of the laser is a linear function of the slit width of the monochromator. The laser-induced fluorescence signal is expected to be a linear function of the slit width of the monochromator if the image of the laser beam is substantially larger than the slit width. This is bound to be the case for the range of slit widths used in our experiment. The use of a spatially constant laser intensity in Ref. 4 for deriving Eq. (1) is consistent with this observation.

Measurement of the laser-induced fluorescence over a wide range of neon-gas pressure is difficult. For given voltages on the electron-gun electrodes the electron-beam diameter depends on the Ne pressure. This dependence on the Ne-gas pressure can arise in the following ways: (i) elastic or inelastic scattering of the electron beam by the Ne atoms, or (ii) space-charge effects produced by the electron beam itself plus space charge due to the electron-ion pairs formed by electron-impact ionization of the ground-state or metastable Ne. The laser-induced fluorescence is found to be a linear function of the Ne pressure up to pressures of 30 mTorr for the $1s_3$ and $1s_5$ metastable levels provided the electron gun is focused to maintain a constant beam diameter at the viewing region. (For the $1s_2$ and $1s_4$ resonance levels the radiation trapping that maintains the excited-level population is strongly dependent on the Ne density and so even if the electron-beam diameter is maintained constant the laser-induced fluorescence is a linear function of the Ne density only over a small range of pressures.) Additional support for the cross sections measured in this manner is provided by the agreement of measurements using this apparatus we have made of the cross sections for $2p$ excitation with previous measurements made by Sharpton *et al.*[1] at a series of pressures and electron-beam currents some of which are much lower than the ones used in our experiments. Further support for the cross sections measured is provided by the agreement of the energy dependence of our measured apparent cross sections for the $1s_3$ and $1s_5$ metastable levels at energies above 80 eV with the energy dependence of the sum of the cascade cross sections measured by Sharpton *et al.*,[1] and by the agreement of our measured energy dependence of the cross sections for excitation to the $1s_2$ and $1s_4$ levels at energies above 200 eV with the sum of the cascade cross sections measured by Sharpton *et al.* plus the adjusted Born cross section.

The electron-beam space charge does not make it difficult to focus the beam to maintain constant beam diameter in the viewing region. We observe experimentally that a constant beam diameter can be maintained. This is probably due to neutralization of the electron-beam space charge by Ne^+ ions. Even at low-electron energies, Ne^+ ions are formed by electron-impact ionization of the metastable-Ne atoms.

The laser-induced fluorescence is found to be a linear function of the electron current density for the range of electron currents (0—500 μA) used in the experiment. For the $1s_3$ and $1s_5$ levels these tests were carried out at the peak of the cross section and at 50 and 80 eV. For the $1s_2$ and $1s_4$ levels these tests were carried out at 50, 100, and 200 eV.

The reproducibility of the energy dependence of the apparent cross sections for all four of the Ne $1s$ levels is $\pm 10\%$, as determined by taking the standard deviation of many measurements. The absolute uncertainty in the apparent cross sections of the $1s_3$ and $1s_5$ metastable levels is primarily due to the uncertainty of the 100-eV cascade cross sections used to normalize the $1s_3$ and $1s_5$ cross sections. The uncertainty in the sum of the cascade cross sections of Sharpton *et al.* is about 15% or less.[1] This results in an uncertainty of $\pm 20\%$ for the apparent cross sections of both the $1s_3$ and $1s_5$ levels. Since $Q_a = Q_a^A - \sum_{j>a} Q_{ja}$, the uncertainty in Q_a arises from both the uncertainty in Q_a^A and the uncertainty in $\sum_{j>a} Q_{ja}$. For both the $1s_3$ and $1s_5$ levels the uncertainty in the direct cross section is $\pm 25\%$, except at the high-energy end where Q_a is the difference between two numbers which are nearly equal to each other. Obviously at energies above 90 eV our method yields no usual information on the direct cross section for the $1s_3$ and $1s_5$ levels. The absolute uncertainty in the apparent excitation cross sections of the $1s_2$ and $1s_4$ levels is due to the sources mentioned for the $1s_3$ and $1s_5$ levels, plus the uncertainty of the calculated Born cross section at 300 eV. The primary uncertainty in the Born cross section arises from the uncertainty in the measured lifetimes. This leads us to assign an error of $\pm 25\%$ to the apparent cross sections and a $\pm 28\%$ error to the direct cross sections for the $1s_2$ and $1s_4$ levels.

B. Comparison with other experimental work

Various methods have been previously used to measure excitation cross sections of the $1s$ levels. In this section we compare our measurements with measurements of other researchers using different methods. We shall first discuss the metastable levels and then the resonant levels. References will also be made to experiments which determine the sum of excitation cross sections for all four $1s$ levels.

An early experiment for measuring the excitation cross section of the $1s_5$ level of Ne was done by Milatz and Ornstein[13] in 1935. In their experiment the number of metastable atoms ($1s_5$) produced by electron impact is determined by monitoring the attenuation of a beam of 6402-Å light ($2p_9$-$1s_5$ emission from a Ne discharge) due to absorption by the $1s_5$ atoms. They reported the energy dependence of the apparent excitation cross section of the $1s_5$ level but without an absolute normalization. They observed a more rapid decrease of cross section with increasing energy than we do as illustrated in Fig. 6. They used a low Ne pressure ($\sim$0.02 Torr) and without the detection apparatus available today, it is possible that they had a serious signal-to-noise problem. Hadeishi[14] used a similar

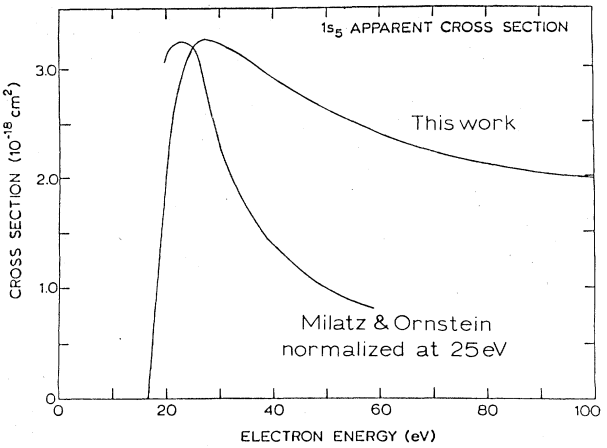

FIG. 6. Comparison of our absolute $1s_5$ apparent excitation cross sections with the relative cross sections of Milatz and Ornstein (Ref. 13) normalized to our value at 25 eV.

method and operated in the pressure range of 0.4—1.7 Torr where secondary processes may occur. His measured cross sections for the $1s_5$ level depend markedly on the pressure and are more than ten times the cross sections we observe. Aside from the difference in absolute magnitude, the energy dependence of Hadeishi's cross sections is also quite different from ours.

Dorrestein's measurements[15] of the sum of the apparent excitation cross sections of the two metastable levels agrees well with our results, in both energy dependence and magnitude. The difficulties of this method include determining the efficiency for the ejection of secondary electrons from the metal surface by an incident metastable atom and separating the contributions to the total secondary electron emission of the metastable atoms and the ultraviolet photons. He took care to overcome these problems. Teubner *et al.*[16] also have measured the sum of the apparent excitation cross sections of the $1s_3$ and $1s_5$ states using a time-of-flight technique. Their measurements are below ours but only by the amount within the span of the uncertainties. The results of the measurement of the sum of the apparent excitation cross sections of $1s_3$ and $1s_5$ are summarized in Table III. Dunning *et al.*[17] measured the ratio of the population of the $1s_3$ and $1s_5$ levels produced by electron impact. They used a laser to selectively remove either the $1s_3$ or $1s_5$ atoms from a beam of metastable atoms and detected the metastable atoms by secondary electron emission from a metal surface. Their measurements give the $1s_3$-to-$1s_5$ ratio at electron energies 35, 60, 80, and 100 eV as, respectively, 6.9 ± 1.4, 5.8 ± 0.6, 5.1 ± 0.4, and 5.0 ± 0.4 which are somewhat larger than our corresponding values of 5.2, 4.6, 4.2, and 4.3 for the apparent excitation cross sections.

Very recently, Register, Trajmar, Steffenson, and Cartwright[18] have reported differential cross sections for excitation of sixteen features in the electron energy-loss spectrum of Ne. By integrating their measured differential cross sections they obtain the total (integral) cross section Q for direct excitation (excluding cascade). As remarked in their paper, the agreement between their $1s_3$ and $1s_5$ cross sections and ours is reasonably good (except at energies above 60 eV for the reasons discussed earlier in this paper). A graphical comparison between the two sets of data is given in Ref. 18.

TABLE III. Comparison of our results of the sum of the apparent electron-impact excitation cross sections of the two metastable levels at different energies with those of Dorrestein (D) in Ref. 15, and those of Teubner, Riley, Tonkin, Furst, and Buckman (TRTFB) in Ref. 16. Cross sections are in units of 10^{-19} cm^2.

	$Q^A(1s_3)+Q^A(1s_5)$		
E (eV)	D[a]	TRTFB[b]	This work[c]
25	43	40	39
30	41	34	37
40	36	29	35
50	33	26	32
60	30	23	29
70	28	21	27
80	26	20	25
90	24	18	24

[a]Estimated uncertainty not given in Ref. 15.
[b]Uncertainty bar about ±14% at 50 eV and ±16% at 100 eV as read from the graph in Ref. 16.
[c]Estimated uncertainty 20%.

For the resonant levels, Hertz[19] measured the apparent excitation cross sections of $1s_2$ and $1s_4$ using the optical method on the vacuum ultraviolet (vuv) emission of the resonance levels. He obtained absolute cross sections by normalizing the neon measurements using previously measured He cross sections. Uncertainties in the values are due to the difficulty in calibrating the detection system as a function of wavelength, and to the imprisonment of the resonance radiation. He reports a pressure-dependent shape of the $1s_2$ excitation functions that he attributes to a reduction of the polarization by resonance radiation trapping. Our measurements, however, show no dependence of the shape of the excitation functions on pressure. We find closer agreement of our $1s_2$ apparent excitation cross section with the "low-pressure" results than the "high-pressure" results of Hertz even though our data were taken at higher gas pressures than the high-pressure data of Hertz. It is not clear to us why there is a discrepancy between Hertz's results and ours. Hertz found no pressure dependence of the shape of $1s_4$ apparent excitation function, and his $1s_4$ cross sections agree well with ours in both magnitude and energy dependence. A comparison for the $1s_2$ and $1s_4$ apparent cross sections is shown in Tables IV and V, respectively.

Tan, Donaldson, and McConkey[20] have measured the $1s_2$ apparent excitation cross section at energies above 100 eV by means of vuv spectroscopy. They use an atomic beam to remove the problems of radiation trapping. For absolute calibration they use the Born-Bethe approximation along with an oscillator strength of 0.132 which is 11% smaller than the one we use (0.147). The energy dependence of their cross sections is in good agreement with ours, but their cross sections are about 35% lower than ours (see Table IV). Tan, Donaldson, and McConkey assumed that the cascade population of the $1s_2$ level

TABLE IV. Comparison of our values of the $1s_2$ apparent excitation cross sections at different energies with those of Hertz (H) obtained at two different pressures ($P_1=27\times10^{-4}$ Torr and $P_2=0.3$–0.8×10^{-4} Torr) as reported in Ref. 19, and with those of Tan, Donaldson, and McConkey (TDM) in Ref. 20. Cross sections are in units of 10^{-18} cm^2.

	$Q^A(1s_2)$			
E (eV)	$H(P_1)$	$H(P_2)$	This work	TDM
100	20	18	12	7.6
150	18	15	10	
200	16	13	8.6	5.6
250	14	11	7.2	
300	13	9.2	6.3	4.4

varies with energy like E^{-1}, whereas we determine the cascade population by direct measurement. As will be seen in the next subsection, the cascade population of the $1s_2$ level has a $(\log_{10}E)/E$ component which amounts to about 20% of the $(\log_{10}E)/E$ term of the direct excitation cross section. This together with the 11% difference in the values of oscillator strength mentioned above accounts for the difference between the cross sections of Tan *et al.* and ours.

Register *et al.*[18] also report total cross sections for direct excitation of the $1s_2$ and $1s_4$ levels obtained by integrating their measurement of differential cross sections. Their results for the $1s_2$ level agree well with ours but the agreement for the $1s_4$ level is much poorer (Fig. 10 of their paper). They suggested that the difference between their integral cross sections and our results may be due to the uncertainties in accurately accounting for the cascade from higher electronic levels at all incident electron energies. However, the experiments of Sharpton *et al.*[1] show that the cascade to the $1s$ levels is overwhelmingly dominated by the $2p\rightarrow1s$ emissions which are accurately measured. Moreover, even if we artificially change the absolute values of the cascade cross section by, say, 30%, the resulting change in the energy dependence of the direct excitation cross sections evaluated from our data is small. Because the cascades are accurately determined we believe they cannot account for the difference between our cross section and the cross section obtained by integrating the differential cross sections of Ref. 18.

Schaper and Scheibner[21] have determined the excitation cross section of Ne in the region of 16–21 eV by the Maier-Leibnitz method,[22] which gives the percentage of inelastic impacts. At electron energies less than the $2p$ excitation threshold, their excitation cross section is the sum of the cross sections of the four $1s$ levels. At an electron energy of 18 eV, they obtain a value of 2.5×10^{-18} cm^2; the sum of our four measured cross sections at 18 eV is 3.3×10^{-18} cm^2. Their measurements are in agreement with ours within the stated uncertainties.

TABLE V. Comparison of our values of the $1s_4$ apparent excitation cross sections at different energies with those of Hertz (Ref. 19). Cross sections are in units of 10^{-18} cm^2.

	$Q^A(1s_4)$	
E (eV)	Hertz	This work
50	3.0	2.9
100	2.4	2.7
150	1.9	2.2
200	1.6	1.9
250	1.4	1.7
300	1.2	1.5

Johnston and Burrow[23] have also measured the total excitation cross section of neon near the excitation threshold. They report a total excitation cross section of 4.2×10^{-18} cm^2 at 18 eV in neon with an uncertainty of $\pm15\%$. It is consistent with our results within the uncertainty brackets.

C. Discussion of the results of cross sections

In Fig. 4 we show the "Bethe plot" for the apparent and direct excitation cross sections of the $1s_2$ and $1s_4$ levels, i.e., the energy dependence of cross sections in the form of Q times E versus $\log_{10}E$. We emphasize the absolute calibration in our measurement of the $1s_2$ and $1s_4$ levels is based on normalization of the measured apparent excitation cross section at 300 eV to the sum of the scaled Born direct excitation cross section plus the experimentally measured total cascade cross section. This differs from the procedure of normalizing the measured cross section to the Born-Bethe formula with the use of the experimental oscillator strength as done in Ref. 24 and other works. Our normalization scheme does not require that the measured cross sections be in the energy regime where the Born-Bethe theory is valid. Nevertheless, it is interesting to examine to what extent the Born-Bethe energy dependence of the cross section is satisfied in the energy range of our experiment. According to the Born-Bethe theory the direct excitation cross section of a dipole-allowed level (DAL) such as the $1s_2$ and $1s_4$ levels has at high incident-electron energy a characteristic energy dependence

$$Q(\mathrm{DAL})=\mathrm{const}\times\frac{\log_{10}(cE)}{E}=\frac{a}{E}+\frac{b\log_{10}E}{E}\ , \qquad (9)$$

where b is proportional to the oscillator strength of the transition between the ground level and the DAL. The cascade population of this level is due to radiation from a series of higher levels such as the $2p$ levels that are dipole forbidden (but spin-allowed) with respect to the ground level. At high energies the $2p$ levels have direct excitation cross sections inversely proportional to the incident energy. The $2p$ levels also receive cascade from such levels as $2s_2$, $2s_4$, $3s_2$, $3s_4$, $3d_5$, $3d_2$, and $3s'_1$ which are dipole allowed with respect to the ground level with direct excitation cross section given by the functional form of Eq. (9) at high energies. The apparent excitation cross section of a $2p$ level therefore contains both a $1/E$ and a $(\log_{10}E)/E$ term, hence the same is true for the $2p\rightarrow1s_2$ cascade cross section. Thus the total cascade cross section to a DAL at high energies may be written as

$$Q_{\mathrm{casc}}(\mathrm{DAL})=\frac{a'}{E}+\frac{b'\log_{10}E}{E}\ , \qquad (10)$$

and the apparent excitation cross section as

$$Q^A(\mathrm{DAL})=\frac{a+a'}{E}+\frac{(b+b')\log_{10}E}{E} . \quad (11)$$

It is interesting to note that all four plots in Fig. 4 show linearity at energies as low as 120 eV. The slopes of the Bethe plots for the apparent and direct excitation cross sections give, respectively, $b+b'$ and b. For the $1s_4$ level Fig. 4 shows a much larger slope for Q^A than for Q. The $1s_4$ level is mostly a $^3P_1$ state with only a 7% $^1P_1$ admixture, whereas the $1s_2$ level has a 93% weighting of $^1P_1$. At high incident energies the $1s_4$ level has a much smaller direct excitation cross section than does $1s_2$. As is evident in Fig. 4, the major part of the apparent cross section for $1s_4$ is due to cascade. The difference in slope between Q^A and Q indicates that the cascade cross section of $1s_4$ contains a component which varies with energy like $(\log_{10}E)/E$. A similar difference in slope exists between Q^A and Q for the $1s_2$ level. The relative slopes m for the four curves in Fig. 4 are $m(Q^A,1s_2)=5.9$, $m(Q,1s_2)=5.0$ $m(Q^A,1s_4)=1.6$, and $m(Q,1s_4)=0.5$. For both the $1s_2$ and $1s_4$ levels, $m(Q^A)$ differs from $m(Q)$ by a similar amount. This is reasonable since we expect $1s_2$ and $1s_4$ to have comparable amount of cascade from the higher levels. Thus $m(Q^A)$ is not equal to the coefficient of the $(\log_{10}E)/E$ term in the Born-Bethe formula for direct excitation as $m(Q^A)$ includes the $(\log_{10}E)/E$ component from both direct excitation and cascade. This is one reason why the $1s_2$ absolute excitation cross sections reported by Tan *et al.* are lower than ours.

Because of the use of the theoretical cross sections for absolute calibration of the experimental data for the $1s_2$ and $1s_4$ levels, comparison of the experimental direct excitation cross sections for these two levels with theory is meaningful only in a limited way. Nevertheless, the experimental direct excitation cross sections for the $1s_2$ and $1s_4$ levels obtained by normalization at 300 eV are in good agreement with the corresponding Born-approximation values down to 150 eV as shown in Ref. 6. The fact that the Bethe plots for the direct excitation cross sections exhibit the same degree of linearity over the same energy range as those for the apparent excitation cross sections is another indication of the internal consistency of our data.

Our experimental results for the $1s_3$ and $1s_5$ cross sections, which do not involve normalization to theoretical values, allow us to test the theoretical calculations. This is especially important as the earlier measurements by Sharpton *et al.* on the excitation of the $2p^53p$, $2p^54p$, $2p^54d$, and $2p^55s$ ($2p$, $3p$, $4d$, and $3s$, respectively, in Paschen's notation) levels do not provide a conclusive comparison between theory and experiment. The main problem there is the lack of sufficiently accurate wave functions for the intermediate-coupling case. While the wave functions of the individual levels can be expanded by the Russell-Saunders-coupling eigenfunctions, calculation of the coefficients of expansion from first principles is difficult. Instead Sharpton *et al.* obtained the coefficients of expansion by the semiempirical method of Cowan and Andrew.[25] The wave functions determined in this manner were useful for discussing the qualitative features of the excitation functions, but the cross sections calculated from these wave functions generally are not expected to be accurate enough for a quantitative comparison with experiment. Some of the levels such as $2p_9$ are purely triplet levels with no singlet admixture. However, for these levels the apparent excitation cross section is dominated by cascade in the energy range where the Born-type approximation is valid. In Ref. 1 much of the cascade into the $2p_9$ level was deduced by combining observed optical cross sections with theoretical transition probabilities. This introduces a significant uncertainty to the results of the direct excitation cross section which were obtained by subtracting the deduced cascade from the measured apparent excitation cross sections. Comparison of theory and experiment for the $2p_9$ level, as discussed in Ref. 1, was rather unsatisfactory.

For the $1s_3$ and $1s_5$ levels we are free of the aforementioned difficulties. Fajen has calculated direct excitation functions for these levels at incident energies of 40—300 eV using the Born-Ochkur approximation.[12] In Table VI we show a comparison of Fajen's theoretical cross sections with the experimental values. Above 60 eV, the measured apparent excitation cross sections are nearly the same as the cascade cross sections. This makes a large uncertainty in the direct excitation cross sections which are obtained as the difference between those two terms. Within the limited energy range covered in Table I, the agreement between theory and experiment is very good. We feel that the agreement at 40 eV is probably better than what one normally expects of a calculation based on the Born-Ochkur approximation along with the Hartree-Fock-Slater wave functions. Nevertheless it is satisfying to see that for these low excited levels for which the wave functions can be well approximated by a pure triplet term from a single configuration, the calculated cross sections reproduce the experimental values well. Recently Machado, Leal, and Csanak[26] have calculated the direct excitation cross sections of the $1s_3$ and $1s_5$ levels by a first-order many-body theory. Their results at 40 and 50 eV are much larger (about a factor of 2) than the Born-Ochkur and our experimental values (see Table I).

We may point out that the ratio of the measured $1s_5$ to

TABLE VI. Comparison of the measured direct excitation cross sections (in 10^{-19} cm^2) of the $1s_3$ and $1s_5$ levels with theoretical values obtained by the Born-Ochkur (BO) approximation and by a first-order many-body theory (FOMBT).

	40 eV	50 eV	60 eV[a]
$Q(1s_3)$, expt.	0.93	0.61	0.42
$Q(1s_3)$, BO	0.91	0.70	0.53
$Q(1s_3)$, FOMBT	2.03	1.26	
$Q(1s_5)$, expt.	4.1	2.3	
$Q(1s_5)$, BO	4.7	3.7	2.7
$Q(1s_5)$, FOMBT	10.16	6.23	

[a]At 60 eV the apparent excitation cross section and the cascade cross section for the $1s_5$ level are so close to each other that the direct excitation cross section, which is obtained by taking their difference, is subject to a large uncertainty.

$1s_3$ direct excitation cross sections is very close to 5 for the entire energy range studied. This conforms to the statistical weight of $2J+1$ for the two levels involved.

V. CONCLUDING REMARKS

Utilizing the technique of laser-induced fluorescence, we have measured the electron excitation cross sections for metastable levels of Ne by means of the optical method. As explained in Sec. II, the laser-induced fluorescence signal $S_{on}-S_{off}$ is directly proportional to the apparent excitation cross section of the metastable level so that a plot of the $S_{on}-S_{off}$ signal versus the incident electron energy gives the relative apparent excitation function. To put it in absolute scale, we make use of the fact that the metastable levels are purely triplet states and most of the levels above them are of mixed singlet and triplet character. The direct excitation cross section of the purely triplet states reaches its maximum value at an incident energy slightly above the threshold and decreases steeply with increasing energy, whereas the mixed states exhibit a much broader maximum in the direct excitation function. At high incident energies (above 80 eV) the apparent excitation cross section of the metastable levels is virtually entirely due to cascade from the higher levels and the contribution from direct excitation is negligible. Since the cascade cross sections to the metastable levels from the higher ones have been measured previously, they are used to provide an absolute calibration for the relative apparent excitation cross sections for the metastable levels. This method of absolute calibration is also applicable to Ar, Kr, and Xe since the same kind of singlet-triplet mixing occurs in the cascading excited states of these atoms.

The use of laser-induced fluorescence is extended to the measurement of excitation cross sections for the resonant levels. Because of resonant radiation trapping, the effective lifetimes of these levels increase greatly with increasing atom number density. At a pressure about 30 mTorr, the $1s_2$ and $1s_4$ resonant levels of Ne are sufficiently "metastable" that we can apply the technique of laser-induced fluorescence to determine their cross sections.

ACKNOWLEDGMENTS

We wish to thank David Rall for his assistance in the preparation of this paper. This work was supported by the U.S. Air Force Office of Scientific Research.

*Present address: Lawrence Berkeley Laboratory, University of California, Berkeley, California 94720.

[1]F. A. Sharpton, R. M. St. John, C. C. Lin, and F. E. Fajen, Phys. Rev. A **2**, 1305 (1970).

[2]See for example, W. L. Nighan, IEEE Trans. Electron Devices ED-28, 625 (1981); D. L. Huestis, R. M. Hill, H. H. Nakano, and D. C. Lorents, J. Chem. Phys. **69**, 5133 (1978).

[3]N. D. Bhaskar and A. Lurio, Phys. Rev. A **13**, 1484 (1976).

[4]M. H. Phillips, L. W. Anderson, and C. C. Lin, Phys. Rev. A **23**, 2751 (1981).

[5]M. H. Phillips, L. W. Anderson, C. C. Lin, and R. E. Miers, Phys. Lett. **82A**, 404 (1981).

[6]R. E. Miers, J. E. Gastineau, M. H. Phillips, L. W. Anderson, and C. C. Lin, Phys. Rev. A **25**, 1185 (1982).

[7]J. O. Phelps, M. H. Phillips, L. W. Anderson, and C. C. Lin, J. Phys. B **16**, 3825 (1983).

[8]F. M. J. Pichanick and J. A. Simpson, Phys. Rev. **168**, 64 (1968).

[9]M. S. Feld, M. M. Burns, T. V. Kuhl, P. G. Pappas, and D. E. Murnick, Opt. Lett. **5**, 79 (1980).

[10]R. M. St. John, F. L. Miller, and C. C. Lin, Phys. Rev. **134**, A888 (1964).

[11]N. F. Mott and H. S. W. Massey, *The Theory of Atomic Collisions,* 3rd ed.(Oxford University, London, 1965).

[12]F. E. Fajen, Ph.D. thesis, University of Oklahoma, 1968.

[13]J. M. W. Milatz and L. S. Ornstein, Physica (Utrecht) **2**, 355 (1935).

[14]T. Hadeishi, Ph.D. thesis, University of California, Berkeley, 1962.

[15]R. Dorrestein, Physica (Utrecht) **9**, 447 (1942).

[16]P. J. O. Teubner, J. L. Riley, M. C. Tonkin, J. E. Furst, and S. J. Buckman, in *Abstracts of Contributed Papers of the XII International Conference on the Physics of Electronic and Atomic Collisions, Gatlinburg, Tennessee, 1981,* edited by S. Datz (North-Holland, Amsterdam, 1981).

[17]F. B. Dunning, T. B. Cook, W. P. West, and R. F. Stebbings, Rev. Sci. Instrum. **46**, 1072 (1975).

[18]D. F. Register, S. Trajmar, G. Steffenson, and D. C. Cartwright, Phys. Rev. A **29**, 1793 (1984).

[19]H. Hertz, Z. Naturforsch **24A**, 1937 (1969).

[20]K.-H. Tan, F. G. Donaldson, and J. W. McConkey, Can. J. Phys. **52**, 786 (1974).

[21]M. Schaper and H. Scheibner, Beitr. Plasma Physik **9**, 45 (1969).

[22]See, for example, H. S. W. Massey and E. H. S. Burhop, *Electronic and Ionic Impact Phenomena* (Oxford University, London, 1969), Vol. 1.

[23]A. R. Johnston and R. D. Burrow, Bull. Am. Phys. Soc. **26**, 1295 (1981).

[24]S. T. Chen and A. C. Gallagher, Phys. Rev. A **17**, 551 (1978).

[25]R. D. Cowan and K. L. Andrews, J. Opt. Soc. Am. **55**, 502 (1965).

[26]L. E. Machado, E. P. Leal, and G. Csanak, Phys. Rev. A **29**, 1811 (1984).